Bank-to-Turn Missile Autopilot Design Using Loop Transfer Recovery

Kevin A. Wise*
McDonnell Douglas Astronautics Company, St. Louis, Missouri

Linear quadratic Gaussian/loop transfer recovery control theory is used to design a bank-to-turn missile autopilot. This paper presents the steps of the design and analysis procedure and demonstrates them in designing a missile autopilot at a single flight condition. Autopilot design issues such as bandwidth, model uncertainty, and noise sensitivity are discussed using singular values of their respective matrix quantities.

Introduction

STABILITY and robustness requirements for current and future asymmetrical bank-to-turn (BTT) missile configurations being proposed for air-to-air and air-to-ground missions necessitate the use of optimally designed multi-input/multi-output (MIMO) digital control systems.[1,2] High-performance robust flight-control system design requirements are generally driven by high-maneuver rates needed for terminal homing. Stability robustness concerns are often related to large launch envelopes and uncertainties in plant dynamics created by conformal and internal carry missile configurations. Recent advances in multivariable control techniques appear to offer promising solutions to this complex MIMO bank-to-turn control problem.

In general, designing autopilots using conventional analytical methods involves iterative single-loop-design analyses that are costly in time and manpower. These classical techniques are misleading in evaluating system stability and robustness concerning model inaccuracies. Missile autopilots are often designed by discretizing the flight envelope at specific points, designing the autopilot at these points, and guaranteeing robustness to parameter variations by designing large single-loop stability margins and evaluating the design through simulation. Recent developments in control system design provide the theoretical mathematics required for optimizing the controller design and evaluating stability and robustness to parameter uncertainties.[3-15] Using new methods for characterizing missile-model uncertainties,[4,7,11] controller robustness properties may be evaluated, reducing the number of design conditions analyzed.

Much recent attention has been directed toward satisfying stability and robustness requirements by designing autopilots using optimal control theory.[16] However, practical application of these techniques in the missile industry has been limited.[17] A major problem in this area is transforming the frequency-domain performance and stability requirements into time-domain requirements and the determination of the robustness of the design to model-parameter uncertainties and unmodeled high-frequency dynamics. A multivariable optimal controller design using a quadratic performance index optimizes the design in the time domain. Satisfying frequency-domain requirements such as bandwidth, noise sensitivity, etc., using the optimization performance index, is a problem. Similarly, quantifying the degree of robustness required to overcome parameter uncertainties is not well defined.

This paper summarizes the design steps for designing a linear quadratic Gaussian (LQG) with loop transfer recovery (LTR) missile autopilot with the loop broken at the plant input. In particular, the linear quadratic regulator (LQR) performance index penalty parameters are chosen to maximize performance and minimize sensitivity. A tradeoff is established between stability robustness recovery (LTR) and sensor noise amplification, which limits the amount of recovery possible.

Missile Dynamics

The nonlinear equations of motion describing missile aerodynamics are linearized in order to form a finite-dimensional linear time invariant (FDLTI) model that can be used to design an autopilot. In this section FDLTI models are presented that are used to design the LQG/LTR autopilot.

Kevin A. Wise is a Lead Electronics Engineer in the Guidance, Navigation, and Control Division of McDonnell Douglas Astronautics Company (MDAC), Missile and Defense Electronics, and Adjunct Professor of Electrical Engineering, Southern Illinois University in Edwardsville. He received his B.S.M.E., M.S., and Ph.D. from University of Illinois. Since joining MDAC, Dr. Wise has been actively involved in the application of modern estimation and control methodologies in navigation and flight-control problems. He has supported programs analyzing optimal guidance laws for terminal homing missiles, digital processing requirements for conventional and factorized Kalman filter algorithms, GPS aided inertial navigation, and multivariable flight control for bank-to-turn missiles. He has also made significant contributions to the autopilot design activity for the HAVE SLICK flight-test program. Dr. Wise is a member of the IEEE and AIAA.

Presented as Paper 88-0336 at the AIAA 26th Aerospace Sciences Meeting, Jan. 11-14, 1988; received March 31, 1988; revision received Sept. 6, 1988.

*Senior Electronics Engineer. Member AIAA.

Figure 1 displays a highly asymmetric air-to-ground BTT missile configuration designed for conformal carry by an advanced fighter aircraft. Aerodynamic analyses of this airframe configuration show that very strong roll-yaw coupling is present. Large roll rates are induced by sideslip angle created primarily by the asymmetry of the vehicle. For this reason, linearized pitch dynamics are separated from linear coupled roll-yaw dynamics. The resulting autopilot design consists of a vertical/pitch acceleration command autopilot and a lateral roll-yaw autopilot in which a roll rate about the velocity vector is commanded.

The important variables defined in Fig. 1 are ($p\ q\ r$), which are body axis roll, pitch, and yaw angular rates, respectively; ($\phi\ \theta\ \psi$) are integrals of ($p\ q\ r$); α is angle of attack; and β is the sideslip angle. The FDLTI flight-control design equations are formed by linearizing the nonlinear aerodynamic equations of motion about a trim condition.

The vertical/pitch FDLTI flight control equations are

$$\dot{A}_z = V_m Z_\alpha q + V_m Z_\delta \dot{\delta}_e + Z_\alpha A_z \tag{1a}$$

$$\dot{q} = (M_\alpha A_z / V_m Z_\alpha) + [M_\delta - (M_\alpha Z_\delta / Z_\alpha)]\delta_e \tag{1b}$$

The variables Z_α, Z_δ, M_α, M_δ, are the dimensional aerodynamic stability derivatives derived from aerodynamic measurements (wind tunnel) of lift and pitching moment.

In addition to Eqs. (1), actuator dynamics are modeled using a damped second-order transfer function, and the integral of pitch rate is included as a state to model gravity. We can write Eqs. (1) and the actuator model dynamics in state-space form as

$$\dot{x} = Ax + Bu \tag{2}$$

$$y = Cx \tag{3}$$

where

$$x = [A_z\ q\ \theta\ \delta_e\ \dot{\delta}_e]^T \tag{4a}$$

$$y = [A_z\ q]^T \tag{4b}$$

$$u = \delta_{ec} \tag{4c}$$

The FDLTI roll-yaw flight-control equations are

$$\dot{\beta} = p\ \sin(\alpha) - r\ \cos(\alpha) + Y_\beta \beta + Y_{\delta a}\delta_a + Y_{\delta r}\delta_r \tag{5a}$$

$$\dot{p} = L_\beta \beta + L_{\delta a}\delta_a + L_{\delta r}\delta_r \tag{5b}$$

$$\dot{r} = N_\beta \beta + N_{\delta a}\delta_a + N_{\delta r}\delta_r \tag{5c}$$

The variables Y_β, $Y_{\delta a}$, $Y_{\delta r}$, L_β, $L_{\delta a}$, $L_{\delta r}$, N_β, $N_{\delta a}$, $N_{\delta r}$ are dimensional aerodynamic stability derivatives derived from aerodynamic measurements of lateral side force and roll and yaw moments. In addition to Eqs. (5), actuator dynamics for aileron and rudder fins are included.

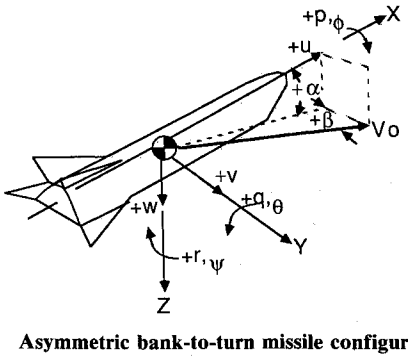

Fig. 1 Asymmetric bank-to-turn missile configuration.

The stability axis coordinate system is defined as the transformation of body axes to the stability axes using angle of attack α. Wind axis coordinate system is defined as the transformation of stability axes to wind axes using sideslip angle β. The missile velocity vector is pointed along the x-axis of the wind coordinate system, as shown in Fig. 1. In a BTT autopilot, induced sideslip is minimized by rolling the missile about the velocity vector. Assuming that beta is very small, this is a rotation about the x-axis in the stability axis coordinate system. Thus, the commanded roll rate is the stability axis roll rate p_s, i.e.,

$$p_s = p\ \cos(\alpha) + r\ \sin(\alpha) \tag{6}$$

The roll-yaw dynamics and fin actuator dynamics are written in state-space matrix form, Eqs. (2) and (3), where

$$x = [\beta\ p\ r\ \phi\ \psi\ \delta a\ \dot{\delta}a\ \delta r\ \dot{\delta}r]^T \tag{7a}$$

$$y = [A_y\ p\ r]^T \tag{7b}$$

$$u = [\delta_{ac}\ \delta_{rc}]^T \tag{7c}$$

The state ϕ is included to model gravity.

The aerodynamics in the FDLTI models are dependent upon several parameters. In this paper a single flight condition is analyzed: Mach = 0.8; altitude = 2000 ft; and a nominal angle of attack = 6 deg.

Linear Quadratic Gaussian With Loop Transfer Recovery Design

Consider the state-space model of Eqs. (2) and (3) where x is the n-dimensional state vector, u is the m-dimensional control vector, y is the q-dimensional output vector, and r is the p-dimensional command input vector where $p < q$ [i.e., dim(r) less than dim(y)]. The robust servo controller design[18] forces p of the q outputs in y to follow r. The output vector y is partitioned as

$$y = \begin{bmatrix} y_c \\ y_{nc} \end{bmatrix} = \begin{bmatrix} C_c \\ C_{nc} \end{bmatrix} x \tag{8}$$

where C_c is a $p \times n$-dimensional matrix, and C_{nc} is a $(q\text{-}p) \times n$-dimensional matrix. The vector y_c contains the controlled outputs and the vector y_{nc} the noncontrolled outputs. The command error is defined as $e = y_c - r$. A new system is created, defined as

$$\dot{z} = \tilde{A}z + \tilde{B}\mu \tag{9}$$

where

$$z = \begin{bmatrix} e \\ \dot{x} \end{bmatrix}, \quad \mu = \dot{u}, \quad \tilde{A} = \begin{bmatrix} 0 & C_c \\ 0 & A \end{bmatrix}, \quad B = \begin{bmatrix} 0 \\ B \end{bmatrix} \tag{10}$$

LQR control theory is applied to Eq. (9) using the PI

$$J = \lim_{T \to \infty} \frac{1}{2T} \int_0^T (z^T Q z + \mu^T R \mu)\, dt \tag{11}$$

The optimal control law for μ using state feedback is formed by solving the algebraic Riccati equation[15] (ARE). The resulting steady-state $m \times (p+n)$-dimensional feedback controller gain matrix K_c is partitioned as

$$K_c = [K_I \quad K_x] \tag{12}$$

where K_I multiplies the integral of the command error vector, and K_x multiplies the states. The optimal control $u(t)$ is obtained by integrating $\mu(t)$, i.e.,

$$u(t) = \int \mu \, dt = -K_c \int z \, dt = -K_I \int e \, dt - K_x x \tag{13}$$

This controller mechanization yields integral control action on the command error to provide zero steady-state error command following. The state vector x must also be available for feedback. When the state vector is not available, it must be estimated using a Kalman filter. This creates the LQG design problem.

The LQR, in addition to generating a minimizing control $u(t)$, provides good stability properties. Provided the optimization problem of Eq. (11) is well posed, the resulting optimal controller guarantees closed-loop stability. This states that using optimal regulator gains, the loop gain remains outside a unit disk centered at the $(-1, j0)$ point in the complex plane (Nyquist diagram). This guarantees a $(-\frac{1}{2} + \infty)$ gain margin and a phase margin greater than or equal to 60 deg.[13,20] If a Kalman filter is used to estimate the state vector for feedback (LQG), these excellent stability properties are no longer present.

The LTR approach of Doyle and Stein[8,9] allows the recovery of the LQR frequency-domain characteristics in the LQG controlled system. This technique has received much recent application.[21-25] The block diagram of Fig. 2 illustrates the robust servo LQG control concept. The frequency-domain properties of the LQG system do not equal the LQR system, primarily due to the observer dynamics introduced by the Kalman filter.

The LQR loop transfer function matrix (LTFM) at the plant input is

$$L_{LQR}(s) = K_c \Phi_{OL}(s) \tilde{B} \tag{14}$$

where

$$\Phi_{OL}(s) = (sI - \tilde{A})^{-1} \tag{15}$$

The LQG LTFM at the plant input is

$$L_{LQG}(s) = K_c \Phi_{KF}(s) K_f C \Phi_{OL}(s) \tilde{B} \tag{16}$$

where

$$\Phi_{KF}(s) = (sI - \tilde{A} + \tilde{B}K_c + K_f C)^{-1} \tag{17}$$

and K_f is the Kalman filter gain matrix. Considering the loop broken at the plant input, LTR modifies K_f to create a system that has stability properties that asymptotically approach those of the LQR. The method uses a trial and error procedure in which the filter design is parameterized by a scalar q^2, such that when $q^2 \to \infty$, we have $L_{LQG}(s) \to L_{LQR}(s)$ asymptotically, but not necessarily uniformly. It is evident that the location of the Kalman filter eigenvalues, Eq. (17), alters the closed-loop frequency characteristics of the system. The LTR procedure systematically recovers the LQR stability and robustness properties by modifying $\Phi_{KF}(s)$. The LQG/LTR approach requires that the controlled system (plant) be minimum phase (i.e., no RHP transmission zeros). The requirement for minimum phaseness occurs because the LTR procedure asymptotically inverts the plant dynamics of the Kalman filter and substitutes the linear regulator dynamics. If there was an RHP transmission zero, an RHP pole would be created, causing an unstable system. The procedure may still be applied to nonminimum phase systems, but care must be taken to prevent instability in the LQG compensator. This limits the amount of recovery.

The LTR procedure consists of designing Kalman filters with the plant process disturbance spectral density matrix Q_f parameterized with a scalar q^2 as

$$Q_f = Q_0 + q^2 \tilde{B} \tilde{B}^T \tag{18}$$

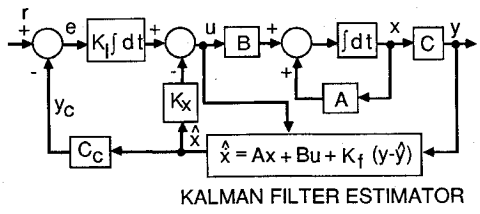

Fig. 2 Robust servo LQG using integral control—estimated state feedback.

where Q_0 is the nominal design, $\tilde{B}$ is the control input distribution matrix, and q^2 is the filter compensation parameter. This parameter is adjusted to recover the LQR frequency-domain characteristics over the frequency range of interest. The modified matrix Q_f is used to compute a steady-state filter gain matrix K_f to be used in the LQG controller of Fig. 2.

The LQG controller design, examining the loop properties at the plant input, may be realized through the synthesis technique:

Step 1: LQR controller design. Design PI weighting matrices Q,R such that the resulting LTFM $L(s) = K_c(sI - \tilde{A})^{-1}\tilde{B}$ meets performance and stability robustness requirements. The frequency-domain properties of the LQG system will be no better than those of the LQR system.

Step 2: Kalman filter design. Design the Kalman filter state estimator using Eq. (18), selecting a filter recovery parameter q^2 that recovers the LQR frequency-domain characteristics over the frequency range of interest. The BTT missile autopilot design problem is solved by performing these two steps.

Step 1: LQR Controller Design

The BTT missile autopilot design, based on separation assumptions, consists of independent pitch and roll-yaw designs. In completing step 1 of this design approach, the LQR PI penalty matrices Q and R must be determined. If the Q matrix is factored as $Q = N^T N$, then the frequency-domain equality for LQR's, derived from the ARE, is

$$[I + L(s)]^H R [I + L(s)] = R + (N\Phi_{OL}B)^H (N\Phi_{OL}B) \tag{19}$$

If $R = \rho I$, then

$$\sigma_i(I + L) = [1 + (1/\rho)\sigma_i(N\Phi_{OL}B)]^{1/2} \tag{20}$$

which shows that the loop gain never enters the unit disk centered at the $(-1, j0)$ point.[20] Thus, choose $R = I$, incorporate ρ into N, and design the elements of the Q matrix to meet performance and robustness requirements. The problem in step 1 is to define an acceptable parameter space for Q by limiting its magnitude using robustness and performance specifications.

The robust servo performance index for the pitch dynamics [Eq. (1)], is defined as

$$J_p = \lim_{T \to \infty} \frac{1}{2T} \int_0^T [q_1(\int e_{Az})^2 + q_2 \dot{\delta}_e^2 + u^2] dt \tag{21}$$

where e_{Az} is the error between commanded and actual vertical body acceleration, $\dot{\delta}_e$ is elevon fin rate, $u = \delta_{ec}$ is commanded elevon fin deflection, and q_1 and q_2 are elements of Q. The elevon fin control law is obtained by solving the robust servo LQR design problem, Eq. (11), which consists of selecting the penalties in Eq. (21). The resulting control law is

$$\delta_{ec} = u = -K_I \int e_{Az} \, dt - K_x x \tag{22}$$

where K_I is a scalar and K_x a 1×5 matrix. The performance index for the roll-yaw dynamics, Eq. (5), is defined as

$$J_{ry} = \lim_{T\to\infty} \frac{1}{2T}\int_0^T [q_3(\int e_{ps})^2 + q_4\beta^2 + \boldsymbol{u}^T\boldsymbol{u}]\mathrm{d}t \qquad (23)$$

where e_{ps} is the error between commanded and actual stability axis roll rate, and $\boldsymbol{u}$ contains aileron and rudder fin deflection commands. The aileron and rudder fin control law is

$$\boldsymbol{u} = -K_I\int e_{ps}\,\mathrm{d}t - K_x\boldsymbol{x} \qquad (24)$$

where K_I is a 2×1 matrix and K_x a 2×9 matrix.

The pitch and roll-yaw autopilots are designed using the PI's in Eqs. (21) and (23). The magnitude of the penalties in the PI alters the performance and robustness characteristics of the closed-loop system. Using the flight condition previously described, the eigenvalues of the closed-loop system $\lambda(A\text{-}BK_c)$ are examined varying the penalties in the PI. There are only two parameters to be varied in the pitch PI design. Figures 3–5 display the eigenvalues of the closed-loop pitch system varying the acceleration error penalty q_1 and actuator fin rate penalty q_2. In Fig. 3, the LQR root locus is shown varying q_1 between 0.0 and 7.0×10^{-3} with $q_2=0.0$. As is the nature of LQR designs, the RHP zero at $+14$ is mirrored into the LHP, and two of the eigenvalues are observed moving toward the zero at -14 as q_1 is increased. In Fig. 4, the actuator fin rate penalty q_2 is varied with $q_1=0.0$. As the penalty on fin rate is increased, the actuator eigenvalues move radially about the origin at a constant spectral radius. The damping of the pair of

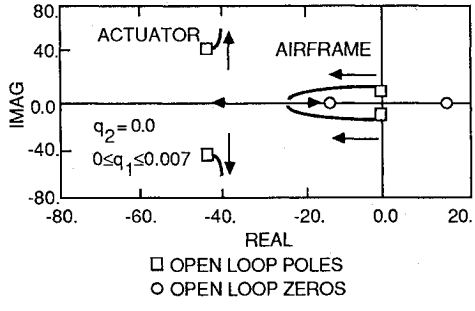

Fig. 3 Pitch LQR root locus with q_2 fixed varying q_1.

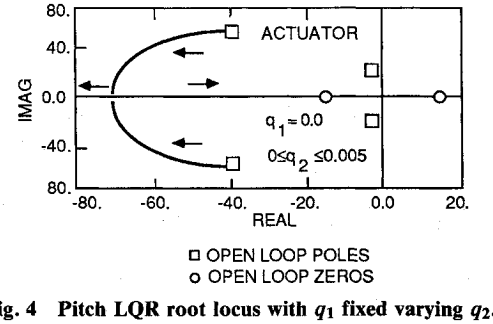

Fig. 4 Pitch LQR root locus with q_1 fixed varying q_2.

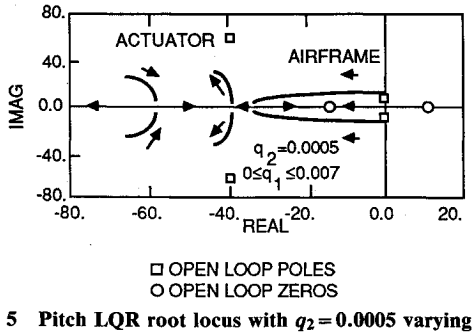

Fig. 5 Pitch LQR root locus with $q_2=0.0005$ varying q_1.

actuator eigenvalues is increased, while the natural frequency is unchanged. Figure 5 displays the root square locus varying q_1 with $q_2=5.0\times10^{-4}$. The actuator eigenvalues move toward the real axis as the acceleration error penalty is increased. The airframe eigenvalues circle the zero at -14 and also become real. They then break away from the real axis at -35 and move outward. The root locus results indicate that several of the closed-loop eigenvalues obtain large negative real parts as the acceleration error penalty is increased.

In the roll-yaw PI design, there are two penalty parameters that are varied in magnitude. This PI design, when analyzed by varying the PI penalties, indicates that the roll and yaw loops are decoupled through the LQR robust servo design process. The closed-loop eigenvalues associated with the roll loop move leftward further into the LHP depending upon the magnitude of q_3 (roll rate error penalty), whereas the eigenvalues associated with the yaw loop move according to the magnitude of q_4 (sideslip penalty). The eigenvalues move in a decoupled fashion because of the observability of the eigenvalues through the pair $(A,Q^{1/2})$. If the eigenvalue is not observable through this pair, then the controller gain matrix resulting from the solution of the ARE will not alter its location.

The PI penalty parameters are selected using design charts created from a frequency-domain analysis of the LQR design. To determine the performance, stability, and robustness in the frequency domain, the singular values of several matrix functions are used. These matrices are defined as:

$L(s)$ = loop-transfer function matrix (LTFM)

$I+L(s)$ = return-difference function matrix (RDFM)

$I+L^{-1}(s)$ = stability-robustness function matrix (SRFM)

The LTFM is analogous to the scalar open-loop transfer function of a single-input/single-output (SISO) system. Also de-

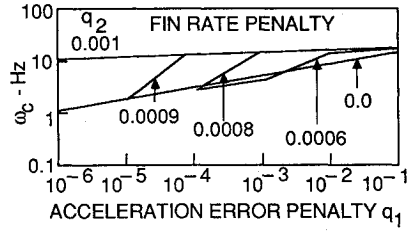

Fig. 6 Pitch performance index design chart—LGCF sensitivity.

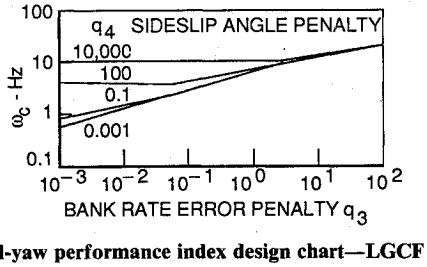

Fig. 7 Roll-yaw performance index design chart—LGCF sensitivity.

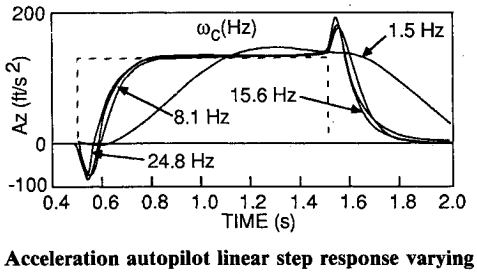

Fig. 8 Acceleration autopilot linear step response varying LGCF.

fined are the RDFM, analogous to the denominator of the closed-loop SISO transfer function, and the SRFM, analogous to the inverse of the scalar closed-loop transfer function. The singular values of the above matrix functions are ordered in size, with $\bar{\sigma}$ denoting the largest and $\underline{\sigma}$ denoting the smallest.

One of the more important autopilot design issues is the bandwidth of the system defined as the loop-gain crossover frequency (LGCF). In the pitch design, the LTFM is scalar. In this case, the magnitude of the loop-gain transfer function (at the plant input) is equated to 1 to determine the LGCF. In the roll-yaw design, the LTFM is a 2×2 matrix where the frequency at which $\bar{\sigma}[L_{LQR}(j\omega)]=1$ is used to describe the LGCF. The eigenvalues of the closed-loop LQR design never move into the RHP. If the open-loop system has RHP transmission zeros, they are mirrored into the LHP, and as the PI penalties become large, the eigenvalues will migrate toward these LHP mirror images. This property of LQR designs, unlike its classical counterpart, guarantees a stable closed-loop system as the PI penalties, or gain magnitude in its classical counterpart, are made arbitrarily large. If we consider the largest spectral radius of the closed-loop system as a measure of the bandwidth, we see that as the PI penalties become large, the bandwidth becomes large. If high-frequency unmodeled dynamics are present, the actual system will be unstable.[16] This important fact must be used to limit the bandwidth so that robustness to unmodeled high-frequency dynamics is ensured. Figures 6 and 7 display the LGCF for the pitch and roll-yaw PI designs. Figure 6 shows how increasing pitch fin rate penalty increases the LGCF. Similarly, Fig. 7 shows the effects of increasing sideslip angle penalty on LGCF for the roll-yaw design using zero aileron and rudder fin rate penalties.

The pitch time-domain performance metric is acceleration command settling time. Figure 8 displays the pitch linear step response using the pitch acceleration command autopilot varying the LGCF. The transfer function relating normal acceleration as the output to elevon fin deflection command as the input contains an RHP zero, as shown in Fig. 3. The undershoot exhibited in Fig. 8 is caused by this RHP zero. The step responses show that as the LGCF is increased from 1.5 to 8.1 Hz, the settling time is greatly improved. As the LGCF is increased further, the return on performance diminishes. Also, as LGCF is increased, the nonminimum phase behavior (undershoot) is amplified.

In roll-yaw the performance metrics are roll-rate command settling time and sideslip angle magnitude. The PI penalty q_3 drives the command settling time. The PI penalty q_4 penalizes sideslip. Linear simulation results commanding a unit step in stability axis roll rate (1 *r/s*) have shown that for sideslip penalties $q_4<0.001$, less than 0.3 deg of sideslip angle is obtained during the roll maneuver. When sideslip angle penalty q_4 is increased to 1.0 less than 0.02 deg, β is obtained. The simulation results (using linear step responses) show that small sideslip angles are obtained for all sideslip penalties examined. The small sideslip angles are obtained because the missile rolls about the velocity vector, not the body roll axis. Using turn coordination minimizes out-of-plane accelerations.

Figure 9 displays the command settling time vs LGCF for the pitch acceleration command and roll-yaw roll rate command autopilots. The settling time T_s is the time required for the commanded variable to achieve and maintain 95% of the commanded value. Since both autopilots use integral control, the steady-state error is zero. Figure 9 demonstrates the diminishing return on T_s as LGCF is increased. Virtually no improvement in T_s is obtained with LGCF's higher than 6 Hz. Using this as a bandwidth limitation, and using Figs. 6 and 7, an upper limit on PI penalty parameter magnitude is defined. From a performance standpoint, the smallest settling time obtainable is best. This would indicate that the PI penalty magnitude should be the largest, as shown in Figs. 6 and 7, without violating the 6 Hz LGCF limit.

One remaining issue still to be evaluated is the sensitivity of the LQR design using these PI penalty magnitudes. Thus far,

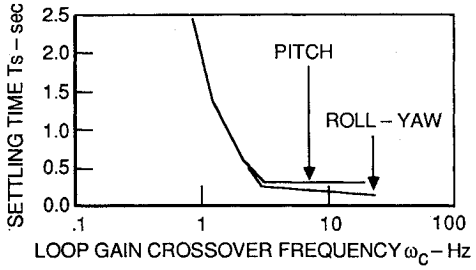

Fig. 9 Performance index design chart—performance sensitivity.

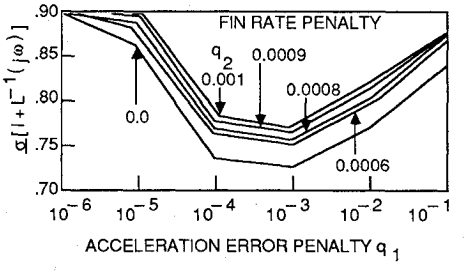

Fig. 10 Pitch performance index design chart—closed-loop sensitivity.

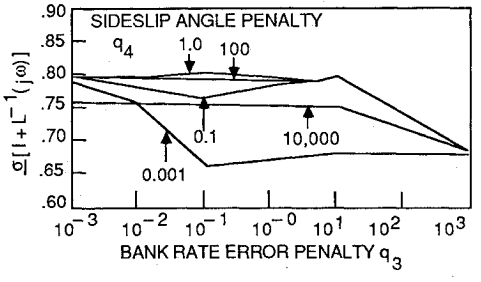

Fig. 11 Roll-yaw performance index design chart—closed-loop sensitivity.

we have used the bandwidth and speed of response to define an acceptable set of PI penalty parameters. The excellent stability characteristic of LQR designs, i.e., $(-\frac{1}{2}, +\infty)$ gain margin, is realized only when there are no unmodeled dynamics. For the LQR design, $\underline{\sigma}$[RDFM] is greater than or equal to unity for all frequencies greater than zero. However, $\underline{\sigma}$[SRFM] does not have this same property. The SISO equivalent of $\underline{\sigma}$[SRFM] is the inverse of the peak resonance. When this is small, the controlled system will exhibit poor tolerance to disturbances, poor tolerance to sensor noise, and poor tolerance to loop-gain variations. Figures 10 and 11 display the LQR $\underline{\sigma}$[SRFM] varying PI penalty parameters. In Fig. 10 the pitch minimum singular value of the stability robustness matrix improves with increasing q_2 given q_1. However, the magnitude of q_2 is limited by the restriction on LGCF, and the improvement obtained in $\underline{\sigma}$[SRFM] with $0.0006<q_2<0.001$ is small. In the roll-yaw design, Fig. 11, the same trend is not observed. For small q_4, $\underline{\sigma}$[SRFM] is small. It then increases with increasing q_4 until $q_4>1.0$, then decreases with increasing q_4. Figure 11 shows that the best $\underline{\sigma}$[SRFM] is obtained when $q_4=1.0$.

Relating performance (settling time) to LGCF, sensitivity ($\underline{\sigma}$[SRFM]) to LGCF, and then LGCF to PI penalty parameter magnitude, the PI penalty parameter magnitudes are selected. For this flight condition they are $q_1=2.5\times10^{-3}$, $q_2=6.0\times10^{-4}$, $q_3=1.7$, and $q_4=1.0$

The LQR PI design process can be summarized as follows: Figs. 6 and 7 relate PI penalty parameters to LGCF. Since each

PI contains two parameters, the Q parameter space is a plane. Figure 9 relates performance to LGCF and shows a constraint on LGCF due to diminishing return on performance. This reduces the plane in the Q parameter space to a line. Figures 10 and 11 relate closed-loop sensitivity ($\underline{\sigma}$[SRFM]) to the Q parameter space. Maximizing $\underline{\sigma}$[SRFM] minimizes closed-loop peak resonance and reduces the line to a single design point.

Step 2: Kalman Filter Design

The goal of LTR is to recover the LQR properties in the LQG design. Inserting the Kalman filter into the feedback loop degrades the stability and robustness characteristics of the LQR design. The LQR property $\underline{\sigma}$[RDFM] ≥ 1 for all $\omega > 0$ is not true for the LQG design, since $L(j\omega)$ is given by Eq. (16). Also, the LQG $\underline{\sigma}$[SRFM] will be smaller than the LQR $\underline{\sigma}$[SRFM].

Loop transfer recovery, as with many design techniques, has penalties associated with its use. The bandwidth of the LQG/LTR compensator increases when recovering the LQR characteristics as $q^2 \to \infty$ in the Kalman filter estimator. However, the compensator bandwidth does not increase beyond the bandwidth of the LQR design. The compensator bandwidth is defined as the frequency at which $\bar{\sigma}[L_{KF}(j\omega)]$ is equal to 1, where

$$L_{KF}(s) = K_c(sI - \tilde{A} + \tilde{B}K_c + K_fC)^{-1}K_f \tag{25}$$

Also, in certain frequency regions sensor noise is amplified. This concern, in particular, establishes a tradeoff that limits the amount of recovery.

Two Kalman filters are designed using the pitch model Eqs. (4) and roll-yaw model Eqs. (7). The numerical values of the plant disturbance spectral density matrix Q_0, Eq. (20), are chosen to cover modeling errors associated with Eqs. (1) and (5). The pitch autopilot uses body measurements of vertical acceleration and pitch rate. The roll-yaw autopilot uses body measurements of lateral acceleration, roll rate, and yaw rate. The 1 σ statistics used to model acceleration and gyro rate measurement noises are 1 ft/s^2 and 0.5 deg/s, respectively. The sensitivity of the Kalman filter design to the Q_0 parameterization was not investigated. This parameterization will impact the LQG/LTR stability robustness since Eq. (8) modifies this matrix. By making key elements in Q_f large, robustness is ensured in the LQG design.

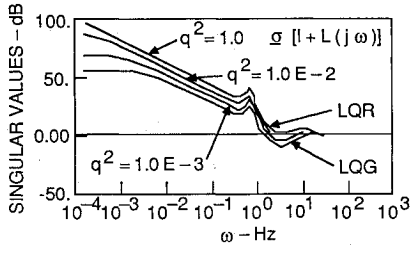

Fig. 12 Pitch RDFM $I + L$ stability robustness recovery using LTR.

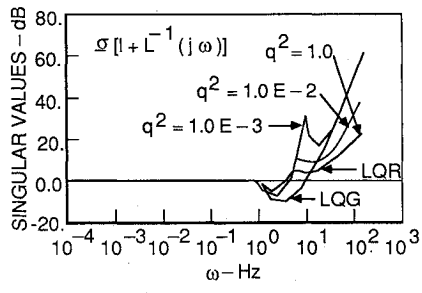

Fig. 13 Pitch SRFM $I + L^{-1}$ stability robustness recovery using LTR.

Figures 12 and 13 display the $\underline{\sigma}$[RDFM] and $\underline{\sigma}$[SRFM] vs frequency of the LQR, LQG, and LQG/LTR designs for the pitch autopilot varying the filter compensation parameter. Comparison of the LQR and LQG $\underline{\sigma}$[RDFM] indicates the degradation in stability associated with the LQG design. Figure 12 shows that the pitch LQG design, processing only measurements of acceleration and pitch rate in the Kalman filter, does not display integral control action. To preserve the integral control action, a measurement of the integral of acceleration error may be processed by the Kalman filter. This raises the order of the compensator to $n + 2p$ $(5 + 2)$, whereas the Kalman filter is of order $n + p$ $(5 + 1)$. If the loop shapes of σ[LTFM] for the LQG/LTR design of order $n + p$ satisfy the low-frequency command following and disturbance rejection requirements, then the addition of the measurement of integral acceleration error is not necessary.

Figures 14 and 15 display $\underline{\sigma}$[RDFM] and $\underline{\sigma}$[SRFM] vs frequency of the LQR, LQG, LQG/LTR for the roll-yaw autopilot varying the filter compensation parameter. As in the pitch design, unless a measurement of the stability axis integral roll rate error is provided to the roll-yaw Kalman filter, the low-frequency integral control acting on roll rate error will be lost.

It is evident from Figs. 12–15 that application of LTR to the LQG design recovers the LQR properties. The amount of recovery is limited by the amount of sensor noise amplification. This means the q^2 cannot approach ∞.

Figures 16 and 17 display $\bar{\sigma}[G(j\omega)]$ where $G(s)$ is the LTFM relating sensor noise in to fin command out. This transfer-function matrix is used to determine if LTR amplifies sensor noise when recovering the LQR properties. These figures indicate that sensor noise will be amplified in both pitch and roll-yaw designs when using large values of q^2. Consider the fin command u generated by the measured output vector $y = Cx + v$, where v represents measurement noise. This relationship is

$$u = -K_c(sI - \tilde{A} + \tilde{B}K_c + K_fC)^{-1}K_f y \tag{26}$$

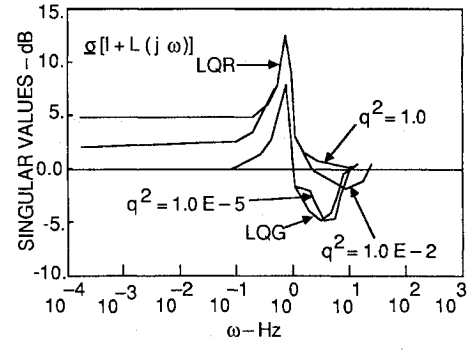

Fig. 14 Roll-yaw RDFM $I + L$ stability robustness recovery using LTR.

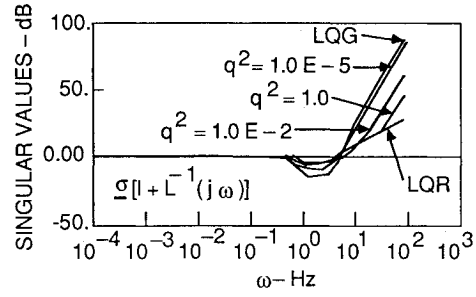

Fig. 15 Roll-yaw SRFM $I + L^{-1}$ stability robustness recovery using LTR.

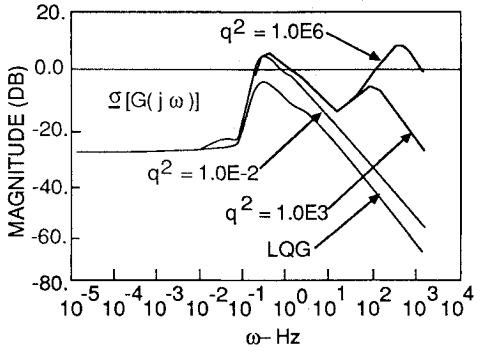

Fig. 16 Pitch LQG compensator sensor noise sensitivity.

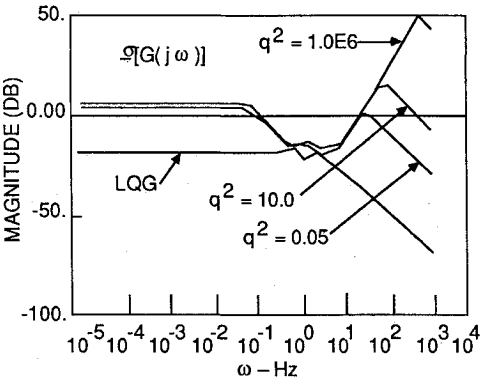

Fig. 17 Roll-yaw LQG compensator sensor noise sensitivity.

Table 1 Pitch and roll-yaw recovery parameters

	q^2	$\underline{\sigma}[I + L(j\omega)]$	Estimator bandwidth (Hz)
Pitch	0.01	0.866	3.20
Roll-yaw	0.05	0.794	0.24

As $q^2 \to \infty$ $K_f \to \infty$, and Eq. (26) can be written as

$$u = -K_c(sI - \tilde{A} + \tilde{B}K_c + K_f C)^{-1} K_f C x - K_c(sI - \tilde{A} + \tilde{B}K_c + K_f C)^{-1} K_f v \quad (27a)$$

$$u \cong K_c x - K_c(sI - \tilde{A} + \tilde{B}K_c + K_f C)^{-1} K_f v \quad (27b)$$

Equations (27) show that $\Phi_{KF}(s)$ cancels $K_f C$ in the first term, and the LQR control law results. The same cancellation is not obtained in the second term, and as q^2 approaches infinity sensor noise will be amplified. The magnitude of q^2 is selected by requiring a minimum singular value gain margin using the RDFM. The minimum value of q^2 that satisfies this requirement is selected since larger values of q^2 amplify measurement noise and increase estimator bandwidth. Using a +12 dB singular value gain margin requirement requires $\underline{\sigma}$[RDFM] > 0.75. Using amplification of measurement noise, RDFM singular value gain margin and estimator bandwidth as guidelines, the filter compensation parameters for pitch and roll-yaw are as shown in Table 1.

Conclusions

A design procedure has been established for applying linear quadratic Gaussian with loop transfer recovery control theory to the design of a bank-to-turn missile autopilot. The problem of choosing linear quadratic regulator performance index penalty parameters is solved through three performance index design charts. These design charts relating performance index penalty parameter magnitude to bandwidth, bandwidth to performance, and penalty parameter magnitude to closed-loop sensitivity systematically designs the state feedback controller. Loop transfer recovery was shown to improve the stability and robustness properties for the estimated state feedback controller implementation. A tradeoff was shown between robustness recovery and sensor noise amplification. This limits the amount of recovery possible.

References

[1]*Proceedings of the Workshop on Bank-To-Turn Controlled Terminal Homing Missiles,* Tactical Weapon Guidance and Control Information Analysis Center, GACIAC PR-85-01, Jan. 1985.

[2]Arrow, A., "An Analysis of Aerodynamic Requirements for Coordinated Bank-To-Turn Autopilots," NASA CR-3644, Nov. 1982.

[3]"Multivariable Analysis and Design Techiques," AGARDograph Lecture Series 117, Oct. 1981.

[4]Lehtomaki, N. A., "Practical Robustness Measures in Multivariable Control System Analysis," Ph.D. Dissertation, Massachusetts Inst. of Technology, Cambridge, MA, 1981.

[5]Doyle, J. C., "Multivariable Design Techniques Based Upon Singular Value Generalizations of Classical Control," AGARD Lecture Series 117, Oct. 1981.

[6]Mukhopadhyay, V. and Newsom, J. R., "A Multiloop System Stability Margin Study Using Matrix Singular Values," *Journal of Guidance, Control, and Dynamics,* Vol. 7, Sept.-Oct. 1984, pp. 582-587.

[7]Doyle, J. C., "Analysis of Feedback Systems With Structured Uncertainties," *Proceedings of the Institute of Electrical Engineers,* Vol. 129, No. 6, Nov. 1982.

[8]Doyle, J. C. and Stein, G., "Robustness with Observers," *IEEE Transactions on Automatic Control,* Vol. AC-24, No. 4, 1979, pp. 607-611.

[9]Doyle, J. C. and Stein, G., "Synthesis of Robust Controllers and Filters," *Proceedings of the IEEE Conference on Decision and Control,* Inst. for Electrical and Electronics Engineers, New York, 1983, pp. 109-114.

[10]Freudenberg, J. S., Looze, D. P., and Cruz, J. B., "Robustness Analysis Using Singular Value Sensitivities," *IEEE Transactions on Automatic Control,* 1981.

[11]Freudenberg, J. S., "Issues In Frequency Domain Feedback Control," Ph.D. Dissertation, Univ. of Illinois, Urbana, IL, 1985.

[12]Safanov, M. G., Laub, A. J., and Hartman, G. L., "Feedback Properties of Multivariable Systems: The Role and Use of the Return Difference Matrix," *IEEE Transactions on Automatic Control,* Vol. AC-26, No. 1, 1981, pp. 47-65.

[13]Lehtomaki, N. A., Sandell, N. R., and Athans, M., "Robustness Results in Linear-Quadratic Gaussian Based Multivariable Control Design," *IEEE Transactions on Automatic Control,* Vol. AC-26, No. 1, 1981, pp. 75-92.

[14]Safanov, M. G., "Stability Margins of Diagonally Perturbed Multivariable Feedback Systems," *Proceedings of the IEEE Conference on Decision and Control,* Inst. for Electrical and Electronics Engineers, New York, 1981, pp. 1472-1478.

[15]Kwakernak, H. and Sivan, R., *Linear Optimal Control,* Wiley, New York, 1971.

[16]Williams, D. E., Madiwale, A. N., and Freidland, B., "Modern Control Theory For Autopilots," Air Force Armament Lab., Eglin AFB, FL, AFATL-TR-85-10, June 1985.

[17]Nesline, F. W. and Zarchan, P., "Why Modern Controllers Can Go Unstable In Practice," *Journal of Guidance, Control, and Dynamics,* Vol. 7, No. 4, 1984, pp. 495-500.

[18]Davidson, E. J. and Copeland, B., "Gain Margin and Time Lag Tolerance Constraints Applied To The Stabilization Problem and Robust Servomechanism Problem," *IEEE Transactions on Automatic Control,* Vol. AC-30, No. 3, March 1985, pp. 229-239.

[19]Doyle, J. C., lecture notes, 1984 ONR/Honeywell Workshop on Advances in Multivariable Control, Minneapolis, MN, Oct. 1984.

[20]Athans, M., "Computer-Aided Multivariable Control System Design," lecture notes, Massachusetts Inst. of Technology, Cambridge, MA, June 1986.

[21]Joshi, S. M., Armstrong, E. S., and Sundararajan, N., "Application of the LQG/LTR Technique to Robust Controller Synthesis for a Large Flexible Space Antenna," NASA TP-2560, Sept. 1986.

[22]Athans, M., Kapasouris, P., Kappos, E., and Spang, H. A., III, "Multivariable Control for the F-100 Engine Using LQG/LTR Methodology," *Proceedings of the AIAA Guidance and Control Conference,* AIAA, New York, 1984.

[23]Ridgely, D. B., Banda, S. S., McQuade, T. E., and Lynch, P. J., "An Application of LQG/LTR To An Unmanned Aircraft," *Proceedings of the AIAA Guidance and Control Conference,* AIAA, New York, 1985; AIAA Paper 85-1927-CP.

[24]Landy, R. J. and Kim, D. B., "Multivariable Control System Design Techniques: An Application to a Short Take Off and Landing Aircraft," *Proceedings of the Sixth Digital Avionics Conference,* Baltimore, MD, 1984.

[25]Youhanaie, M., "Application of Multivariable Control Theory to Improve Steering and Propulsion Control of a Containership," Ph.D. Dissertation, Univ. of Illinois, Urbana, IL, 1984.